Electronic Supplementary Information

Robust Superhydrophobic $V_2O_5/CoFe_2O_4@SiO_2$/PDMS Composite Membrane for Membrane Distillation

Swarnamayee Behera[a], Kalyan Raidongia[b,*] and K. K. R. Datta[a,*]

[a]*Functional Nanomaterials Laboratory, Department of Chemistry, Faculty of Engineering and Technology, SRM Institute of Science and Technology, Kattankulathur, 603203, Tamil Nadu, India*
[b]*Department of Chemistry, Indian Institute of Technology, Guwahati, Assam 781039, India*

Email: kumarard@srmist.edu.in, k.raidongia@iitg.ac.in

Number of pages: 25

Number of figures: 17

Number of tables: 5

Number of references: 21

1. Materials

All the chemicals and solvents with reagent grade quality were purchased commercially and used without any further purification. Nylon microfiltration membrane (pore sizes: 0.2, 0.45, 0.8 μm) was obtained from Axiva Sichem Pvt. Ltd. and PTFE microfiltration membrane (pore size: 0.22 μm) was purchased from Sterlitech Co., USA. SYLGARD™ 184 PDMS Silicone Elastomer Kit was obtained from Dow Chemical Company. Ferric chloride hexahydrate (97%), cobalt chloride hexahydrate (99%), vanadium pentoxide (AR, 99.5%), sodium borohydride, sodium chloride (AR, 99.9%), sodium dodecyl sulphate (AR, 99%) and hexane (99%) were purchased from Siscon Research Laboratories Pvt. Ltd. Bis[3-(triethoxysilyl)propyl] tetrasulfide, S 22.3% (typical) was purchased from Thermo Scientific, tetraethyl orthosilicate from Sigma Aldrich, sodium hydroxide from Fisher Scientific, ethylene glycol and hydrogen peroxide from Qualigens, hexadecane from Spectrochem, and ethanol from Analytical CS reagent.

2. Characterization

Membrane surface morphology was measured by Scanning electron microscopy (FEI, Quanta 200) with energy dispersive X-ray (EDX) analysis. Attenuated total reflectance Fourier transform infrared spectroscopy (ATR-FTIR) spectra were recorded on (Shimadzu IR Tracer-100) to characterize the chemical structure of the prepared powder sample and membranes. The samples were placed on the sample holder and all spectra were recorded from 4000 cm^{-1} to 400 cm^{-1}. The membrane thickness was measured using a thickness gauge (Mitutoyo, 0-25mm) with an accuracy of 1 μm. Thermogravimetric analysis of membranes was carried out with TGA 4000 PerkinElmer instrument with a heating rate of 10^{o}C/min under nitrogen atmosphere. Inductively coupled plasma optical emission spectrometer (ICP-OES) (Model: iCAP 7600, Make: Thermo Fisher Scientific) was used for determination of the concentration

of iron metal present in the permeate solution. Atomic force microscope (AFM, Park Systems Corporation, XE7) was employed to measure the surface roughness of the composite membrane.

Static and dynamic water contact angles were measured by a contact angle goniometer (sessile drop) KYOWA DMs-40, using half-angle method fitting and by FAMAS add-in software with the solvent droplet range of 0.5–2 μL on the membrane's surface. Water contact angles with at least 5 different positions at a membrane surface were tested and the average value was taken as the final contact angle value. Advancing contact angle (θ_A) and receding contact angle (θ_R) were determined by gradually increasing and decreasing the droplet volume on the membrane surface, respectively, to assess surface wettability and hysteresis.

2.1. Surface Free Energy

The surface free energy (SFE) of the membranes was assessed via the extended Fowkes model, also referred to as the Kitazaki-Hata theory.[1-2] By partitioning the SFE majorly into three components including dispersive, polar, and hydrogen bonding this model offers a comprehensive picture of molecular interactions of the solid surface. The SFE of the material is equal to the sum of the dispersive, polar and hydrogen bonding components.

$$\gamma^{total} = \gamma^{d} + \gamma^{p} + \gamma^{h}$$

γ^d = dispersive component, γ^p = polar component, γ^h = hydrogen bonding component

Contact angles were measured using three solvents with varied polarities and surface tensions including water (~72.8 mN/m), ethylene glycol (~47.7 mN/m), and hexadecane (~27.6 mN/m)] at 25°C on the composite membranes. Using the measured contact angle values and applying the Kitazaki-Hata equation, the dispersive, polar, and hydrogen bonding components of the surface energy were calculated. The extracted values are summarized in Table S2.†

2.2. Porosity calculation

Porosity (ε) of the membranes were evaluated by using the gravimetric method.[3] In brief, membrane specimens with a size of 1.5 x 1.5 cm^2 were cut from each membrane, weighed, and then immersed in isopropanol for 25 seconds. Afterward, each square was taken out, gently dabbed on tissue paper to remove surface residue, and weighed again to determine the mass of the liquid absorbed by the pores. The membrane porosity was then calculated by using the following equation

$$\varepsilon = \frac{\frac{W_w - W_d}{\rho_i}}{\frac{W_w - W_d}{\rho_i} + \frac{W_d}{\rho_p}} \times 100$$

Where W_w and W_d represent the weight of wet and dry membranes (g), respectively, ρ_i is the density of isopropanol in g/cm^3, and ρ_p represents the polymer density in g/cm^3.

2.3. Liquid entry pressure

The LEP of the composite membranes was determined using a custom-made setup. Initially, the membrane was placed in a sealed membrane filter holder (Stainless Steel Filter Holder, dia-25 mm). Deionized water was poured onto the membrane holder, followed by connected to an N_2 gas cylinder. A barometer positioned between the cylinder, and the holder allowed for precise pressure measurement. The pressure was gradually increased until the first water drop appeared, and this pressure was recorded as the LEP of the membrane. This process was repeated three times and the average value was reported as the final LEP.

2.4. Stability tests

The thermal, mechanical and chemical stability of the BV-CS-P was investigated under extreme conditions including hot saline water (70°C) for 144 h, sonication for 90 min, and acidic (HCl solution, pH = 1) and basic (NaOH solution, pH = 14) conditions at room

temperature for 3 h respectively and a sequential acid-base soaking for 4 h. The water contact angle of the membrane was then measured at room temperature.

2.5. Nano indentation-Mechanical test

The surface hardness (H) and elastic modulus (E) of the membranes were precisely determined through depth-sensing nanoindentation using a Nios Scanning Nanohardness Tester (Ostec Instruments, Moscow, Russia) equipped with a high-precision Berkovich pyramidal indenter. Prior to testing, the membranes were mounted onto glass substrates using water and left to dry at room temperature. Measurements were conducted in a load-controlled mode following a four-step procedure.[4-5] Initially, a certain preload force was applied to establish contact between the indenter and the membrane surface. Once contact was confirmed, the load was increased at a constant rate of 500 μN/s until reaching the maximum force over a span of 10 seconds. This peak load was held steady for 5 seconds to allow deformation to stabilize. The final stage involved unloading the sample at the same rate used during loading. Throughout the process, the instrument continuously monitored both the applied force and the displacement of the indenter to ensure precise and reliable data acquisition. Each membrane sample was tested with seven separate indentations to assess measurement repeatability.

The surface hardness (H) of a material, typically defined as the mean pressure exerted under the nanoindenter, can be calculated using the following equation:

$$H = \frac{P_{max}}{A} \qquad eq.(1)$$

Where P_{max} is the maximum applied force and obtained directly from the load-displacement curve, and A is the projected contact area of the indenter's tip with the Nylon and BV-CS-P membranes.

The initial slope of the unloading segment of the curve (*dP/dh*) is used to determine the indentation modulus (*M*) of the material via the following relation:

$$S = \frac{dp}{dh} = \beta \frac{2}{\sqrt{\pi}} M\sqrt{A} \qquad eq.(2)$$

Here, β is a correction factor based on the geometry of the nanoindenter tip. A Berkovich indenter was used in this study, with β value of 1.034.

The elastic modulus (E) of the material can then be calculated from:

$$\frac{1}{M} = \frac{1 - v^2}{E} + \frac{1 - v_i^2}{E_i} \qquad eq.(3)$$

where ν is the Poisson's ratio of the sample, and E_i and ν_i are the Elastic modulus and Poisson's ratio of the indenter tip, respectively.

Using equations (1)–(3), both the hardness (H) and elastic modulus (E) of the Nylon and BV-CS-P membranes has been determined.

3. Membrane distillation performance

The desalination performance of BV-CS-P and other composite membranes were performed using the custom-made DCMD setup with an effective membrane area of 4.9 cm^2. The membrane was placed in a customized DCMD module. Each side of the membrane, one support mesh (1 mm thick) was used to hold the membrane in a planar shape and reduce the membrane deformation due to the pressure difference between feed and permeate flow. Feed saline water was heated at 70^oC by the heating circulator (HWC 110, Borg Scientific) and circulated to the DCMD module using the inbuilt circulator with a constant flow rate of 92 ml/min. The permeate side temperature was maintained at 20^oC using a refrigerated water bath circulator (CRC 105, Borg Scientific). Four types of saline solutions including 0.3 g/L, 3.5 g/L, 7 g/L NaCl, and sea water (Besant Nagar beach, Tamil Nadu, India) were used to measure the MD performance. Additionally, the salt solution made from 3.5 g/L NaCl is mixed with 35 mg/L SDS and 100 mg/L rust (prepared by precipitation of [$Fe(OH)_3$] using 100 ml of 3 M of

NaOH and 1 M of $FeCl_3$) [$Fe(OH)_3$] respectively were tested to study the anti-fouling and anti-scaling properties. To ensure uniform dispersion and simulate real time fouling conditions, $Fe(OH)_3$ was subjected to 30 min. sonication in distilled water before use in the anti-scaling tests. The conductivities of feed and distilled water were measured in an interval of half an hour by the conductivity meter (HI2003-02, Hanna Equipments), while salt rejection was calculated using the following equation.

$$Salt\ Rejection\ (\%) = \left(1 - \frac{C_p}{C_f}\right) \times 100\%$$

Where C_p and C_f is the concentration of NaCl in permeate and feed side.

Two temperature and pressure sensors were integrated to measure the liquid temperature and pressure at feed and permeate side respectively. One digital flow meter (FTB336D, Omega) and one mount panel flow meter (FL50003A-V, Omega) were installed in the pipelines to continuously monitor the flow rate in the feed and coolant loops.

The flux generated from the direct contact membrane distillation performance was recorded in an interval of half an hour and calculated from the equation

$$Flux\ (J_w) = \frac{Q}{\Delta t \times A}$$

Where Q = increase in water in permeate side (litre), Δt = operation time interval (h), A=effective membrane area (m^2).

4. Characterization of CS ($CoFe_2O_4$ @ SiO_2)

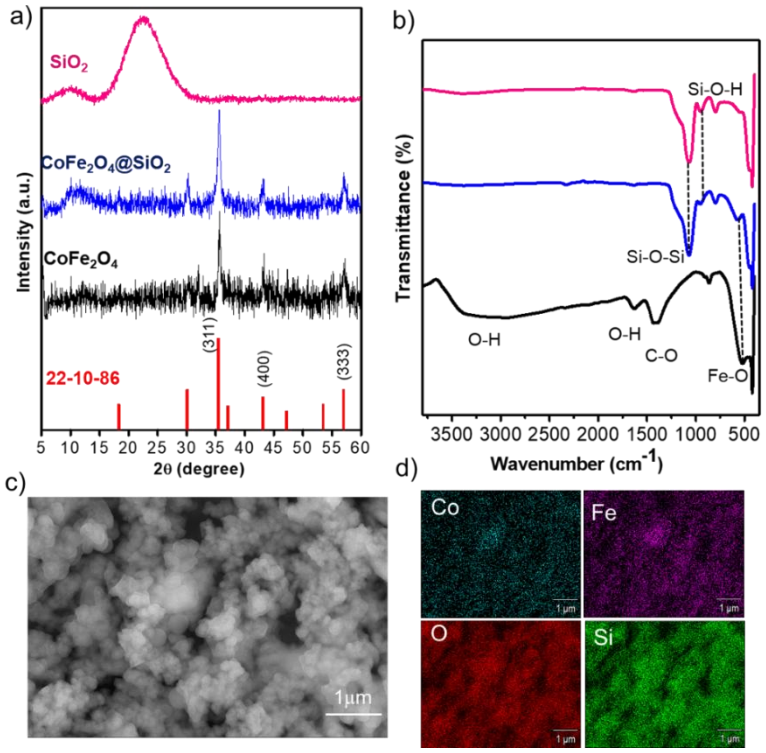

Fig. S1. (a) XRD patterns and (b) FTIR spectra of $CoFe_2O_4$, $CoFe_2O_4$@SiO_2 (CS) and SiO_2 (c) SEM image and corresponding (d) elemental mapping of CS.

5. Characterization of V_2O_5 -TESPT

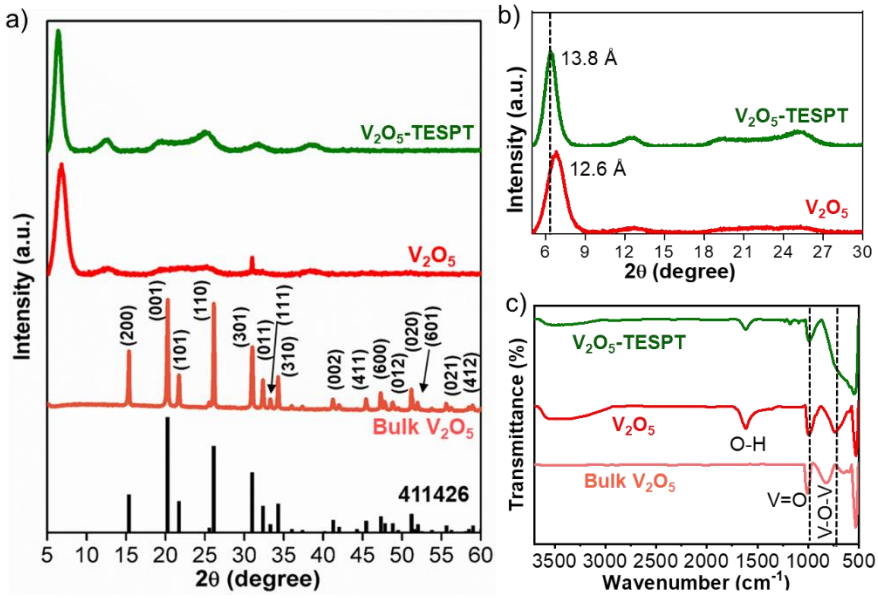

Fig. S2. (a) & (b) XRD patterns and c) FTIR spectra of bulk V_2O_5, V_2O_5 (V_2O_5 nanosheets) and V_2O_5 –TESPT.

Table S1. Components used in composite membrane fabrication.

Sl. No.	**Abbreviation**	**V_2O_5 –TESPT (mg)**	**CS (mg)**	**P (ml)**
1	P(1)(0.45)	-	-	1
2	BV-P(1-1)(0.45)	1	-	1
3	BV-CS-P(1-5-1)(0.2)	1	5	1
4	BV-CS-P(1-2-1)(0.2)	1	2	1
5	BV-CS-P(1-5-1)(0.45)	1	5	1
6	BV-CS-P(1-2-1)(0.45)	1	2	1
7	BV-CS-P(1-5-1)(0.8)	1	5	1

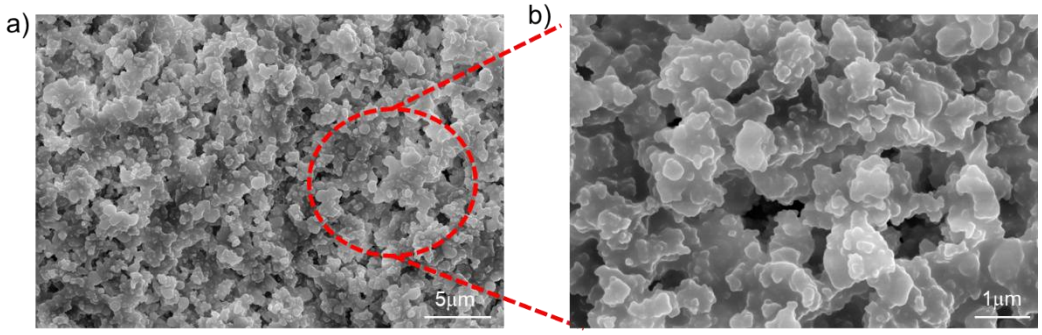

Fig. S3. (a) & (b) SEM images of BV-CS-P(1-5-1)(0.45) at different magnifications.

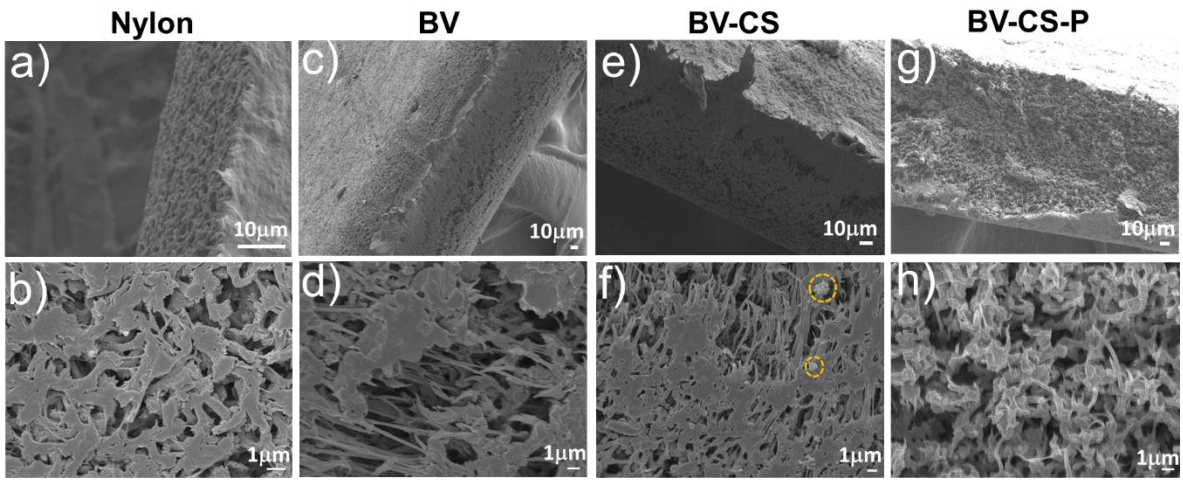

Fig. S4. Cross-sectional SEM images of membranes at low (top row) and high (bottom row) magnifications.

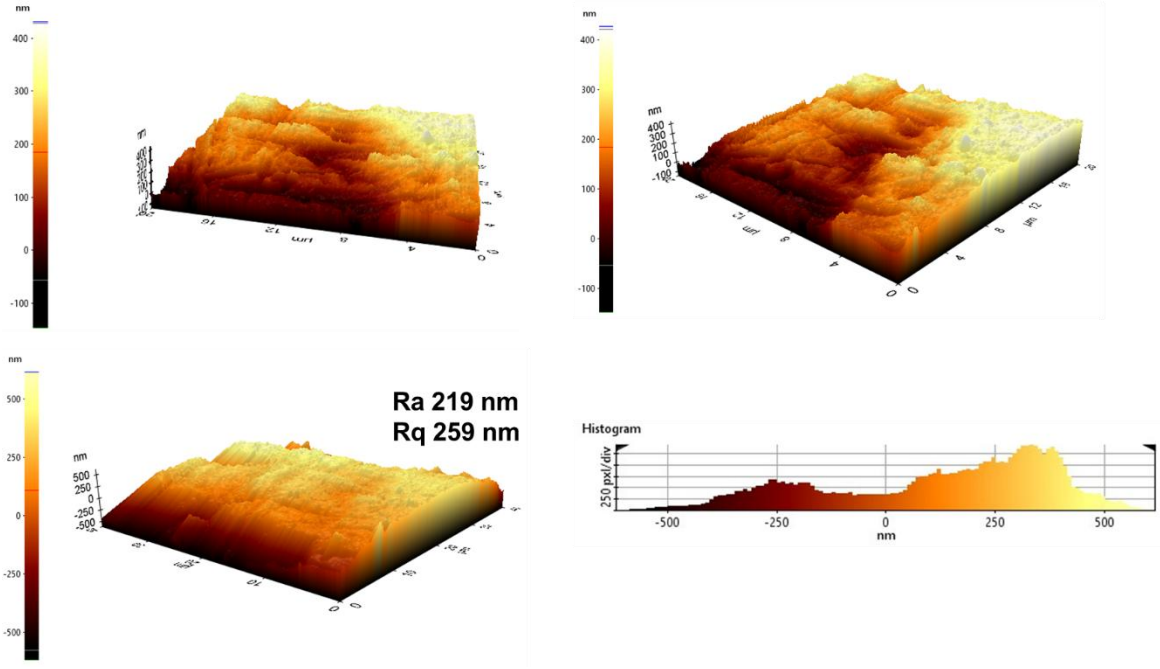

Fig. S5. AFM images, height profile and roughness parameters of BV-CS-P(1-5-1)(0.45).

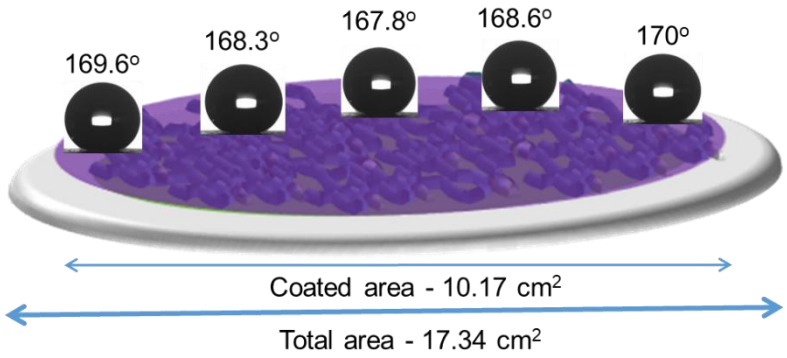

Fig. S6. Water contact angle (WCA) taken across the BV-CS-P(1-5-1)(0.45).

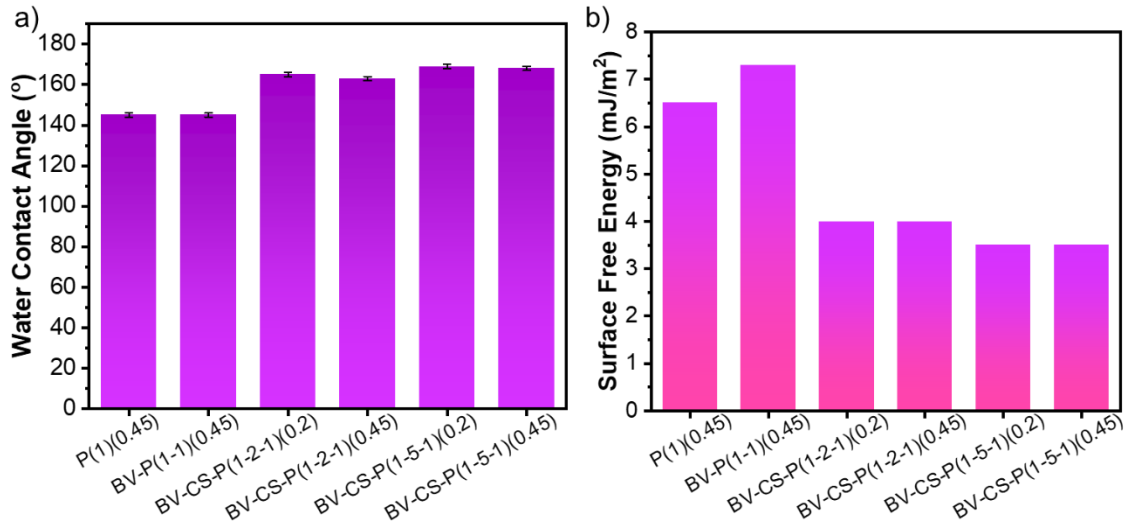

Fig. S7. (a) WCA and (b) corresponding surface free energy of composite membranes.

198 Table S2. Solvent contact angles and surface free energy parameters of various composite

199 membranes.

Solvents / Membranes	Water	Ethylene glycol	n-hexadecane	S.F.E (mJ/m^2)
BV-CS-P (1:5:1)(0.45)	168±1° 	152° 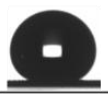	10° 	3.5
BV-CS-P(1:5:1)(0.2)	169±1° 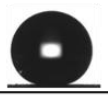	153° 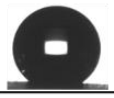	10° 	3.5
BV-CS-P (1:2:1)(0.45)	163±1° 	147° 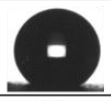	10° 	4
BV-CS-P (1:2:1)(0.2)	165±1° 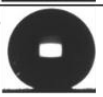	145° 	12°	4
BV-P(1-1)(0.45)	145±1° 	125° 	14° 	7.3
P(1)(0.45)	145±1° 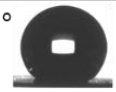	132° 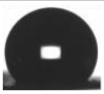	13° 	6.5
BV-CS-P (1:5:1)(0.45) backside	145±2° 	61° 	16°	18.4
BV(1)(0.45)	76±3° 	47° 	17° 	34
Bare nylon (0.45)	31±1° 	29° 	12° 	201.8

200

201 Table S3. Advancing (θ_A), receding (θ_R) contact angle and contact angle hysteresis (θ_{CAH}) of

202 the BV-CS-P(1-5-1)(0.45) taken during the stability test in hot saline water.

Time (hr)	**θ_A (°)**	**θ_R (°)**	**θ_{CAH} (°)**
0	168.8	168.8	0
24	168.8	168.2	0.6
48	167	166.2	0.8
72	16.4	163.2	1.2
96	164.6	161.6	3
120	166.7	158.4	8.3
144	163.8	151.3	12.5

203

6. TG Analysis

The effect of PDMS coating on the thermal stability of the BV-CS-P was investigated using thermogravimetric analysis (TGA). Thermal stability has always been the key to long–term stable use of MD membranes. As shown in Fig. S8, three weight loss were observed. The first weight loss at 35 ºC to 300 ºC (9.15% for BV-CS and 3.64 % for BV-CS-P was mainly owing to the elimination of the water molecule adsorbed on the membrane. The inhibition of water desorption from the PDMS-coated membrane could be ascribed to a high water barrier property of the hydrophobic PDMS coating. The degradation observed at 350 ºC to 650 ºC can be ascribed to the pyrolysis of the functional groups of the polymer. For instance, the weight loss of PDMS non-coated BV-CS membrane is 88.4 % whereas the PDMS coated membrane can be estimated as 75.6%. This suggests that the interactions between the silica coated cobalt ferrite and the PDMS functionalities effectively promote thermal stability. The last stage (0.11 % for BV-CS and 19.11 % for BV-CS-P) was the decomposition of polymer backbones.

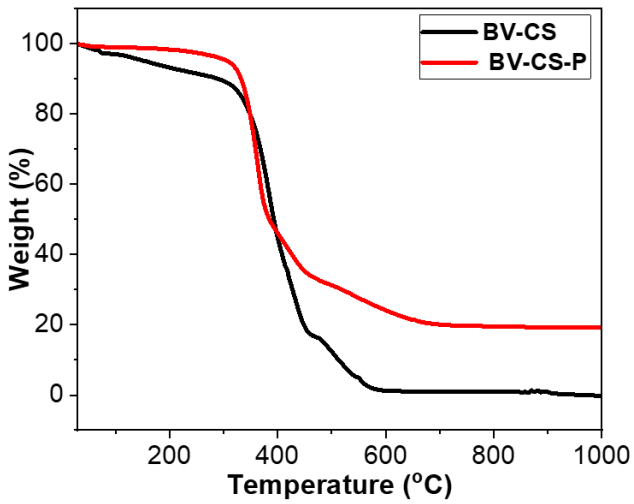

Fig. S8. TG analysis of the composite membrane conducted before and after PDMS modification.

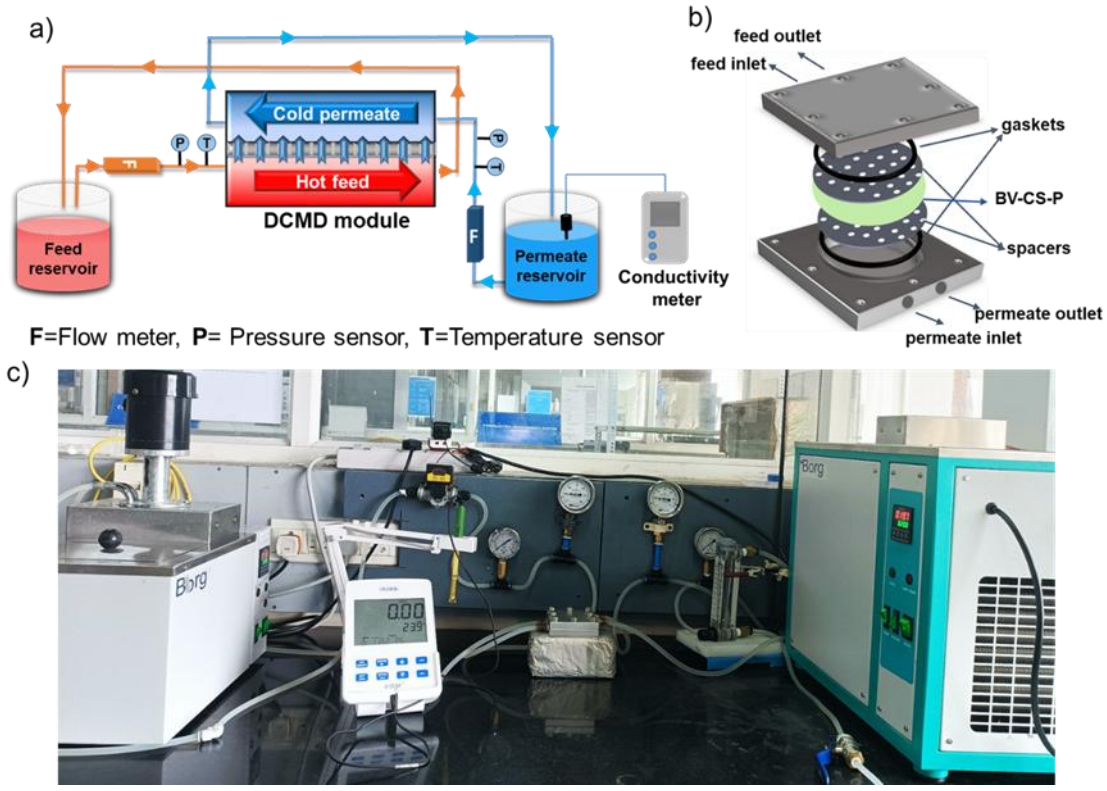

Fig. S9. (a) Schematic representation of the Direct Contact Membrane Distillation (DCMD) setup, (b) 3D diagram illustrating the layout of the DCMD module and (c) photograph of DCMD testing setup.

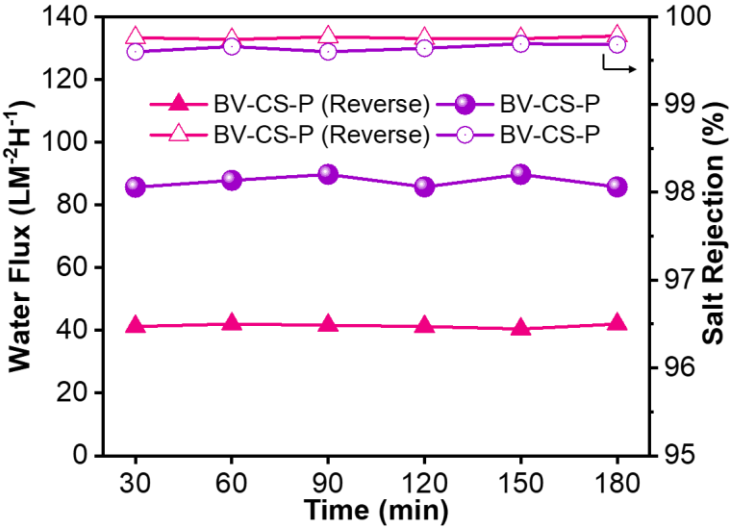

Fig. S10. Comparison of water flux (closed symbols) and salt rejection (open symbols) of BV-CS-P in the standard and reverse orientation configurations.

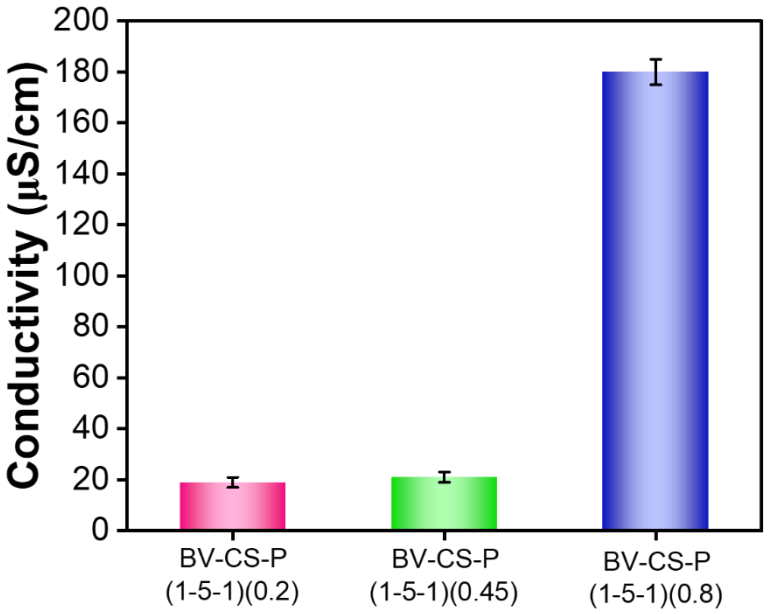

227

228 Fig. S11. Comparison of the permeate conductivity with respect to substrate pore size.

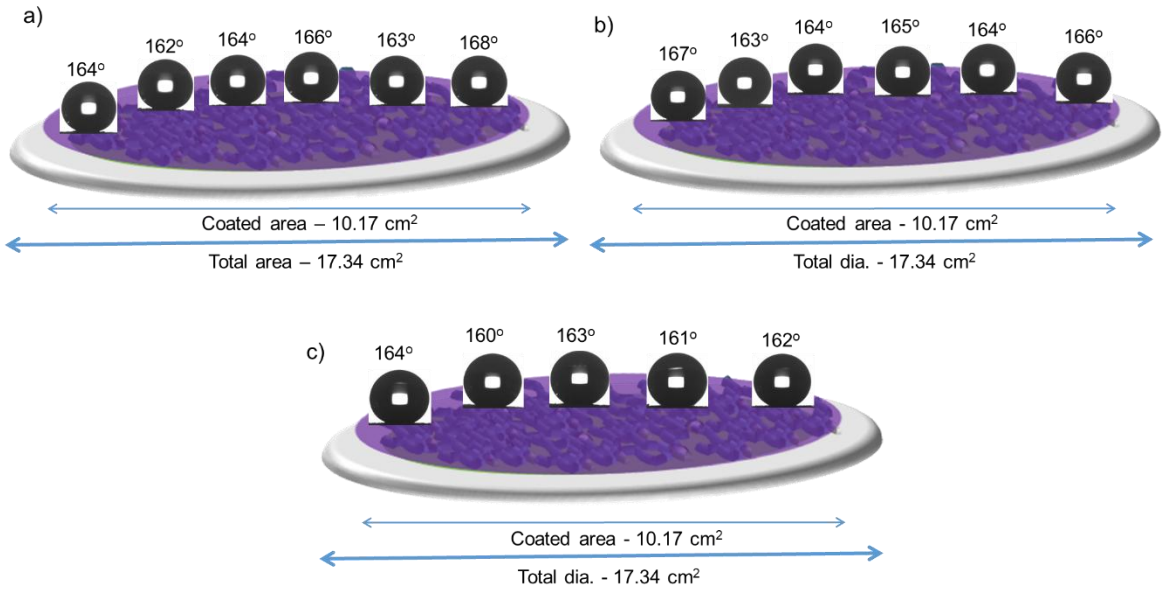

229

230 Fig. S12. WCA across the BV-CS-P(1-5-1)(0.45) after treatment with (a) 3.5 g/L, (b) 7 g/L

231 NaCl and c) sea water as feed solution.

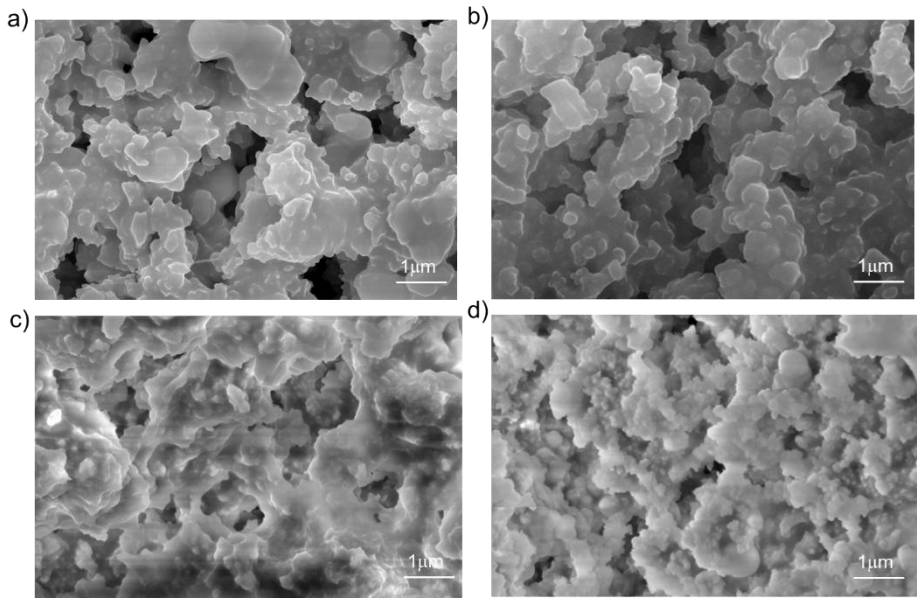

232

233 Fig. S13. SEM images of untreated and recovered BV-CS-P(1-5-1)(0.45) after treatment with
234 various salt concentrations. (a) Untreated, (b) 0.58 g/L, (c) 3.5 g/L, (d) 7 g/L NaCl as feed
235 solution.

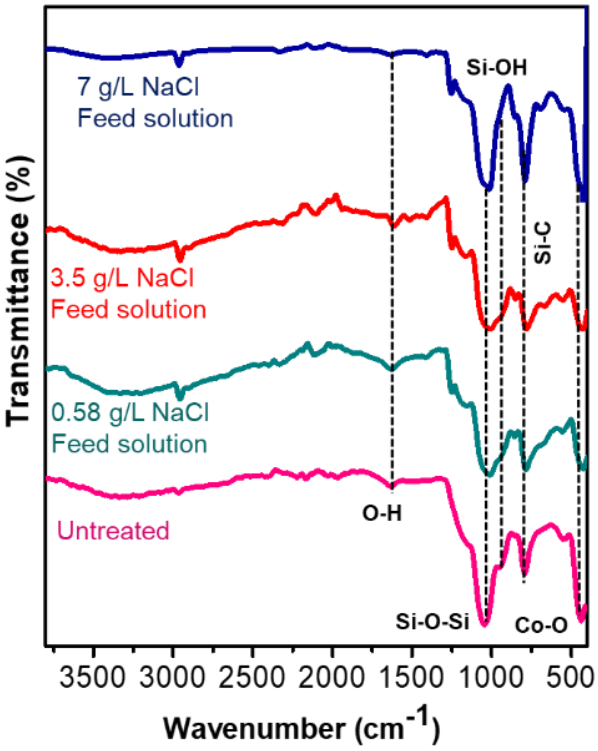

236

237 Fig. S14. FTIR spectra of recovered BV-CS-P(1-5-1)(0.45) after treatment with various salt
238 concentrations as feed solution with respect to the untreated membrane.

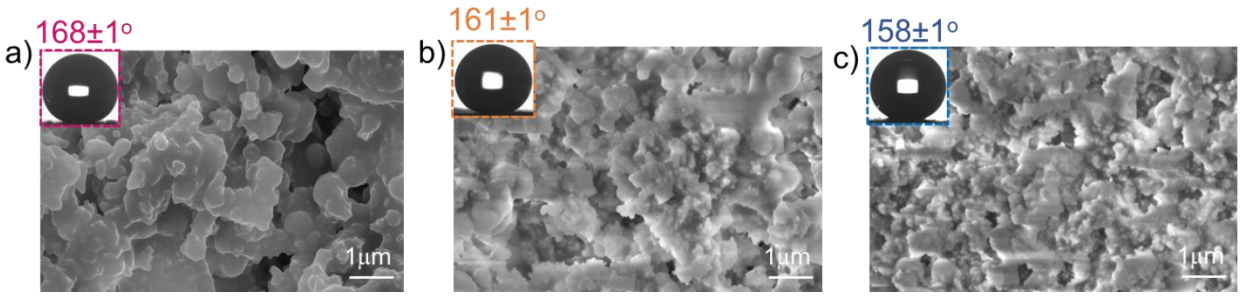

Fig. S15. SEM image and corresponding WCA of untreated and recovered BV-CS-P(1-5-1)(0.45) after treatment with foulants. (a) Untreated, (b) rust, and (c) SDS with NaCl as feed solution.

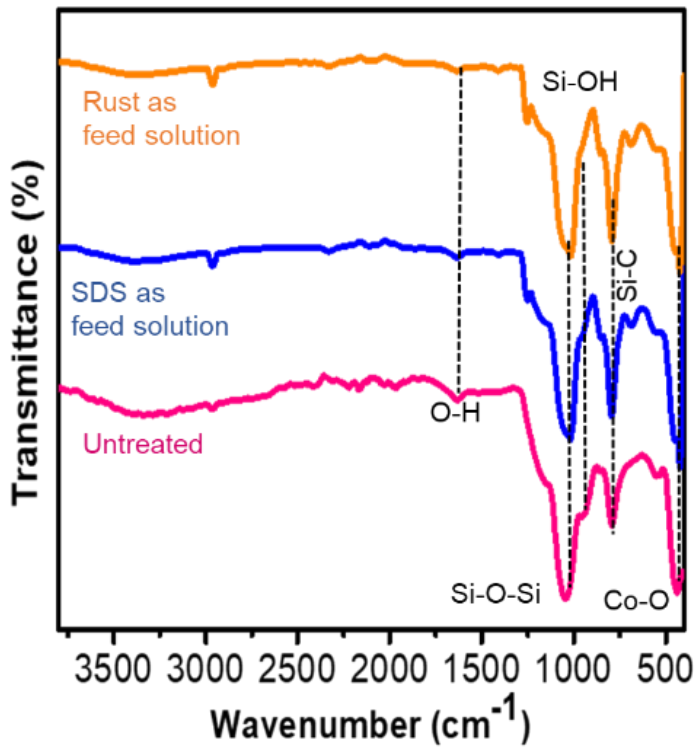

Fig. S16. FTIR spectra of recovered BV-CS-P(1-5-1)(0.45) with respect to the untreated membrane after treatment with SDS and rust with NaCl as feed solution.

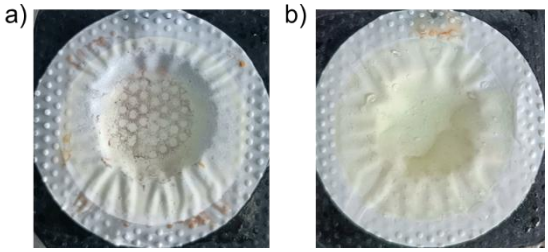

Fig. S17. Digital images of the BV-CS-P(1-5-1)(0.45) before and after water flushing, following membrane distillation of a saline solution containing rust [$Fe(OH)_3$].

Table S4. Comparison of the membrane distillation performance of BV-CS-P with the state-of-the-art hydrophobic membranes using PDMS as the polymer and surface modifier.

Sl. No.	**Fabrication process**	**WCA**	**MD Configuration**	**Operational Parameters**	**Performance**		**Ref.**
					Flux (LMH)	**Rejection**	
1	Electrospinning of PAN followed by heat-pressing at 140◦C: **PAN** Electrospinning of PH (PVDF-HFP) over PAN: **PH-PAN** Electrospraying PS/PDMS over PH-PAN: **PH-PS/PDMS**	148°	DCMD	3.5 wt% NaCl, 70 ◦C, 10 ◦C Area-22.7 cm^2 Flow rate-0.55 L/min	27	~100 %	[6]
2	Electrospinning of PVDF: **PVDF** Polymerization of aniline over PVDF for 30 min: **PANi@PVDF** Immersion of PANi@PVDF in 17-FAS, PDMS for 12 h : **F/Si–PANi@PVDF**	155°	DCMD	3.5 wt% 45 °C. Area -16 cm^2	28	99%	[7]

3	Electrospinning of PVDF: **PVDF** Electrospraying of premixed PVDF, PVDF/ PDMS and SiO_2 solution over PVDF: **PDMS-3**	170º	DCMD	3.5wt % NaCl, 60 ◦C, 20 ◦C Area- 28 cm^2 Flow rate-0.5 L/min	28	99.9%	[8]
4	Electrospinning of PVDF: **PVDF ENM** Immersion of PVDF ENM in PDMS, triethoxyvinylsilane, and ditin butyl dilaurate solution followed by heating at 80°C for 12 h : **Composite ENM**	148°	VMD	3.5 wt% NaCl, 80 °C, Area-19.63 cm^2 Flow rate-130 mL/min	35	99%	[9]
5	Dip-coating of PES substrate (0.2 µm) in APTES followed by heating at 60°C for 5 min. Immersion in silica NPs (5−15 nm) solution, and dried at 60°C for 1 h. Filtration of PDMS and FAS, dried at 60°C for 7 h: **PDMS-FAS/SiNP**	131°	DCMD	1 M NaCl 60 ◦C, 20 ◦C Flow rate-600 mL/s 300 mL/s Area-8.6 × 3.6 cm^2	29	99.9%	[10]
8	**PVDF-PDMS** membrane using NIPS method. Dip-coating in Tollens' reagent followed by air drying for 12 h: **Ag/PVDF-PDMS** Membrane activated with Pd and reduced using hydrochloric acid:	85º	VMD	3 wt% NaCl, 80 ºC Flow rate-80 L/h	5.5	99.9%	[11]

	Ag/a-PVDF-PDMS						
7	Immersion of PVDF substrate (0.22μ m) in catechol and PEI solution, then drying at 45◦C overnight: **PCPA/PVDF** In-situ growth of Ag nanoparticle over PCPA/PVDF in silver nitrate and PVP followed by drying at 45ºC: **Ag/PCPA/PVDF** Immersion of Ag/PCPA/PVDF in PFDT at 30◦C for 24 h then drying at 45ºC : **F-Ag/PCPA/PVDF** Treating F-Ag/PCPA/PVDF with PDMS followed by heating at 120◦C for 2 h : **PF-Ag/PCPA/PVDF**	151º	DCMD	3.5 wt% NaCl 60◦C and 20◦C Flow rate-0.9 L/min Area- 63.59 cm^2	17.6	99.9%	[12]
8	Immersion of electrospun polyimide in dopamine and PEI solution: **PDA/PEI** Deposition of SiO_2 NPs (30 nm) over PDA/PEI: **PDA/PEI-SiO_2** Soaking PDA/PEI-SiO_2 in **17**-FAS and PDMS precursor followed by heating at 120ºC: **RSHO**	158◦	DCMD	20 wt% NaCl, 55ºC and 20◦C Flow rate-100 mL/min Area-9 cm^2	25.4	100%	[13]

9	Immersion of PVDF substrate (0.45 μm) in PDMS and cured at 70◦C for 12 h: **PDMS-PVDF** Polymerization of dopamine over PDMS-PVDF: **PDA-PVDF** Coating of PDA-PVDF with PEI: **PEI-PVDF** Filtration of MXene over PEI-PVDF followed by drying at 70◦C for 3 h: **MXene-PVDF**	130◦	DCMD	0.4 mM SDS in 1.5 wt% NaCl, 100 ppm soybean oil in 1.5 wt% NaCl 80 ◦C and 12 ◦C Area-15.9 cm^2	9.3, 9.1	99.9%	[14]
10	Filtration of V_2O_5-TESPT over nylon substrate (0.45μm): **BV** Roughness creation by depositing $CoFe_2O_4$@SiO_2 NPs (CS) over BV: **BV-CS** PDMS (P) coating on BV-CS followed by drying at 120ºC for 2 h: **BV-CS-P**	168º	DCMD	3.5 g/L NaCl 70ºC and 20◦C Sea water (~ 45,000 μS/cm) 35 mg/L SDS in 3.5 g/L NaCl 100 mg/L rust in 3.5 g/L NaCl Flow rate-93 mL/min Area-4.9 cm^2	87 82 90 83	99.4-99.8 %	**Our work**

Table S5. Comparison of the membrane distillation performance of BV-CS-P with the state-of-the-art hydrophobic membranes made via vacuum filtration route.

Sl. No.	Fabrication Process	WCA	MD configuration	Operational Parameter	Performance		Ref.
					Flux (LMH)	Rejection	
1	Electrospinning of PVDF followed by hot pressing: **PVDF** Filtration of PP solution over PVDF: **PP/PVDF-60**	156º	DCMD	3.5 wt% NaCl 80ºC and 20°C 0.6 L/min 30 cm^2	135.3	99.9%	[15]
2	Polymerization of dopamine over PTFE substrate (0.3 μm**): P-PTFE** Filtration of Fe_3O_4 NPs over P-PTFE: **Fe/P-PTFE** Polymerization of dopamine over Fe/P- PTFE: **P/Fe/P- PTFE**	25º	VMD	6.98 wt.% 65°C 120 L/h 0.012 m^2	18.3	99.9%	[16]
3	Electrospinning of PVDF followed by hot pressing: **PVDF** Filtration of PP solution over PVDF: **PP/PVDF-58**	157º	DCMD	2 wt% NaCl 60ºC 0.6 L/min 12cm^2	53.9	99.9%	[17]
4	Filtration of PDA NPs over PVDF substrate (0.38μm): **PDA-PVDF** Dip coating of PDA-PVDF in PDMS followed by heating at 120ºC for 2 h:	162º	VMD	3.5 wt% NaCl 75◦C 12 cm^2 10 L/h	19	99.9%	[18]

	PDMS-PDA-PVDF						
5	Dip-coating of PES substrate (0.2 μm) in APTES followed by heating at 60°C for 5 min. Immersion in silica NPs (5−15 nm) solution and drying at 60°C. Filtration of PDMS and FAS, dried at 60°C for 7 h: **PDMS-FAS/SiNP**	131°	DCMD	1 M NaCl 60◦C and 20◦C 600 mL/s 300 mL/s 8.6 × 3.6 cm^2	29	99.9%	[10]
6	Reduction of GO to rGO microspheres. Filtration of rGO microspheres (2 μm) and PTFE nanorods (100-200 nm) mixed with Nafion over nylon substrate (0.45 μm), followed by drying at 60°C for 4 h: **Wrinkled rGO microsphere−PTFE**	142°	VMD	3.5 wt% NaCl 50°C 30 L/min 12.57 cm^2	35.7	99.7%	[19]
7	Filtration of GO with silica NPs (400-500 nm) over PAN substrate followed by grafting of HDTMS and heating at 80ºC for 4 h: **hGOM4**	120°	VMD	3.5 wt% NaCl 60°C 120 L/hr	13.5	99.9%	[20]
8	Filtration of GO substrate (1μm): **GOM** Air spraying of TMOS and	150º	AGMD	hydrogen isotopic water separation	0.036	-	[21]

	FTMS-modified silica over GOM. Spray coating of 17-FTMS and MTMOS followed by drying at 70°C for 2 h: **3L-40F**						
9	Filtration of V_2O_5-TESPT over nylon substrate (0.45μm): **BV** Roughness creation by depositing $CoFe_2O_4@SiO_2$ NPs (CS) over BV: **BV-CS** PDMS (P) coating on BV-CS followed by drying at 120°C for 2 h: **BV-CS-P**	168°	DCMD	3.5 g/L NaCl 70°C, and 20◦C Sea water (~ 45,000 μS/cm) 35 mg/L SDS in 3.5 g/L NaCl 100 mg/L rust in 3.5 g/L NaCl Flow rate-93 mL/min Area-4.9 cm^2	87 82 90 83	99.4-99.8%	**Our work**

7. References

1 Y. Kitazaki, T. Hata, *J. Adhes.*, 1972, **4,** 123-132.

2 K.-Y. Law, H. Zhao, Determination of Solid Surface Tension by Contact Angle, in: K.-Y. Law, H. Zhao (Eds.), Surface Wetting: Characterization, Contact Angle, and Fundamentals, Springer International Publishing, 2016pp. 135-148.

3 S. Leaper, E. O. Avendaño Cáceres, J. M. Luque-Alled, S. H. Cartmell, P. Gorgojo, *ACS Appl. Polym. Mater.*, 2021, **3,** 1854-1865.

4 S. Lee, B. G. Choi, D. Choi, H. S. Park, *J. Membr. Sci.*, 2014, **451,** 40-45.

5 G. Pharr, W. Oliver, *J. Mater. Res.*, 1992, **7,** 1564-1583.

6 S. Li, L. Li, J. Zhong, R. Ma, X. Xu, H. Wu, Y. Yu, *Desalination,* 2022, **539,** 115950.

7 L. Zhong, Z. Zhu, Y. Han, Q. Wang, D. Liu, F. Cui, B. Li, W. Wang, *Environ. Sci. Nano,* 2019, **6,** 2553-2564.

8 Y. Liao, G. Zheng, J. J. Huang, M. Tian, R. Wang, *J. Membr. Sci.*, 2020, **601,** 117962.

9 L. Jiao, K. Yan, J. Wang, S. Lin, G. Li, F. Bi, L. Zhang, *Desalination,* 2020, **476,** 114210.

10 A. A. Khan, M. I. Siyal, C.-K. Lee, C. Park, J.-O. Kim, *Sep. Purif. Technol.*, 2019, **210,** 20-28.

11 D. Yue, Y. Wang, H. Zhang, D. Sun, B. Li, X. Ye, W. Fang, M. Liu, *J. Membr. Sci.*, 2021, **638,** 119718.

12 Z. Wei, Y. Jin, J. Li, L. Jia, Y. Ma, M. Chen, *Desalination*, 2022, **529,** 115649.

13 Z. Zhu, L. Zhong, T. Horseman, Z. Liu, G. Zeng, Z. Li, S. Lin, W. Wang, *J. Membr. Sci.*, 2021, **620,** 118768.

14 X. Yan, C. Yang, C. Ma, H. Tao, S. Cheng, L. Chen, G. Wang, X. Lin, C. Yao, *Chemosphere*, 2022, **307,** 136114.

15 L. Deng, P. Li, K. Liu, X. Wang, B. S. Hsiao, *J. Mater. Chem. A*, 2019, **7,** 11282-11297.

16 W. Zhang, S. Yu, P. Li, X. Ji, R. Ning, P. Li, *Sep. Purif. Technol.*, 2023, **313,** 123465.

17 L. Deng, K. Liu, P. Li, D. Sun, S. Ding, X. Wang, B. S. Hsiao, *J. Membr. Sci.*, 2020, **598,** 117813.

18 C. Li, W. Liu, J. Mao, L. Hu, Y. Yun, B. Li, *Sep. Purif. Technol.*, 2023, **304,** 122182.

19 C. Lai, H. Wang, Z. Qu, S. Cheng, H. Fan, H. Meng, *Ind. Eng. Chem. Res.*, 2024, **63,** 12574-12581.

20 Y. Mao, Q. Huang, B. Meng, K. Zhou, G. Liu, A. Gugliuzza, E. Drioli, W. Jin, *J. Membr. Sci.*, 2020, **611,** 118364.

21 M. Wen, M. Chen, K. Chen, P.-L. Li, C. Lv, X. Zhang, Y. Yao, W. Yang, G. Huang, G.-K. Ren, S.-J. Deng, Y.-K. Liu, Z. Zheng, C.-G. Xu, D.-L. Luo, *J. Membr. Sci.*, 2021, **626,** 119136.